Heterogeneity and Relaxation Dynamics of the Photoexcited Retinal Schiff Base Cation in Solution

ARTICLE *in* THE JOURNAL OF PHYSICAL CHEMISTRY B · MARCH 2009

Impact Factor: 3.3 · DOI: 10.1021/jp8077216 · Source: PubMed

3 AUTHORS:

Goran Zgrablić
Sincrotrone Trieste S.C.p.A.
25 PUBLICATIONS **477** CITATIONS
SEE PROFILE

S. Haacke
University of Strasbourg
121 PUBLICATIONS **1,705** CITATIONS
SEE PROFILE

Majed Chergui
École Polytechnique Fédérale de Lausanne
392 PUBLICATIONS **6,503** CITATIONS
SEE PROFILE

Heterogeneity and Relaxation Dynamics of the Photoexcited Retinal Schiff Base Cation in Solution

Goran Zgrablić,[†] Stefan Haacke,[‡] and Majed Chergui*[,§]

Ecole Polytechnique Fédérale de Lausanne, Laboratoire de Spectroscopie Ultrarapide, ISIC, Faculté des Sciences de Base, BSP, CH-1015 Lausanne-Dorigny, Switzerland, Sincrotrone Trieste Elettra, S.S. 14 km 163.5 in Area Science Park, 34012 Basovizza, Trieste, Italy, and Institut de Physique et Chimie des Matériaux de Strasbourg, UMR 7504 CNRS-ULP, 67034 Strasbourg Cédex, France

Received: August 30, 2008; Revised Manuscript Received: December 17, 2008

We present steady-state and broadband femtosecond fluorescence spectra of the protonated Schiff base of retinal in various protic and aprotic solvents, as a function of the excitation wavelength. A detailed spectral decomposition of the time-resolved fluorescence spectra allows us to isolate three spectral components: (i) the vibrationally relaxed S_1 fluorescence, (ii) a vibrationally hot S_1 fluorescence, and (iii) a higher-lying emission that undergoes spectral evolution on a time scale of 300−400 fs, which we assign to S_2 fluorescence. The vibrationally "cold" S_1 fluorescence exhibits three decay components upon 400 nm excitation (except in acetonitrile, which has two), but only two of them upon 570 nm excitation. These components clearly demonstrate the heterogeneity of the S_1 state in the sense that emission stems from several shallow potential surface minima. We discuss a connection between these decay channels and reactive and nonreactive excited-state paths on the basis of their solvent-dependent population and of previous high-performance liquid chromatography studies. There is no clear trend of the fluorescence decay times with solvent properties. Rather, a solvent effect manifests itself in acetonitrile, in that the number of fluorescence decay channels is smaller and that the quenching of the hot fluorescence seems more efficient. This effect has to do with the population pathways leading to the fluorescent states. These observations stress the heterogeneity of excited retinal Schiff base, influencing the decay but also the population channels. They also reinforce the claim that steric effects play an important role in the dynamics of the protein.

Introduction

All-trans retinal is the photosensitive chromophore in many bacterial forms of retinal proteins such as bacteriorhodopsin (bR) and sensory rhodopsin II found in *halobacterium salinarum*.[1] These proteins are important, relatively small model systems for trans-membrane proton/ion pumping and for bacterial photosensors involved in phototaxis. Ultrafast trans−cis photoisomerization of the retinal chromophore is an important premise of the protein function, and it has thus extensively been studied by femtosecond (fs) pump−probe and fluorescence spectroscopy.[2−9]

The protein environment plays a central role in the efficiency and selectivity of isomerization. Indeed, in bR the isomerization occurs selectively around the C_{13}═C_{14} double bond, at a yield of 65%, whereas in solution the yield is low (<20% in most solvents) and the isomerization is highly nonselective.[10−12] A 12−18 D dipole moment change occurs in retinal upon vertical excitation,[13−15] and even larger values are observed in bacteriorhodopsin.[16,17] It has been suggested that the sudden polarization of the protein pocket induces an ultrafast dielectric response of the environment[18−20] and may drive the isomerization dynamics, whereas others have suggested that the "catalytic" action of the protein is determined by steric effects, among others, the presence of charged residues (Arg82, Asp85, and Asp212) in the vicinity of retinal.[21−25]

The study of the ultrafast events in the retinylidene chromophore (protonated Schiff base of retinal, PSBR) has long been used as the benchmark for the understanding of environment effects, by comparison with the protein and the solvents. Such studies have been carried out using ultrafast transient absorption spectroscopy in the visible, near-infrared,[26,27] and mid-IR.[28] Ultrafast fluorescence offers the advantage of connecting the excited-state and the ground-state surfaces only, thus rendering the observations simpler, in principle. We recently reported a study of the ultrafast fluorescence of the retinylidene chromophore, with a resolution of ≤120 fs, as a function of solvent properties, such as viscosity, dielectric constant, and heat conductivity, in order to identify the environment effects that play a role in the dynamics, and to disentangle intramolecular from intermolecular contributions.[29] The spectral evolution of the fluorescence of all-trans PSBRs was recorded in protic (methanol, MeOH; 1-octanol, OctOH; and 2-propanol, ProOH) and nonprotic (cyclohexane, cHex; and dichloromethane, DCM) solvents. The fluorescence exhibited a triexponential decay with time constants ranging from 0.5 to 6 ps. The main observation was that these features were literally independent of solvent despite the more than 1 order of magnitude difference in dielectric constant and/or viscosity between the various solvents. This lack of sensitivity to the properties of the environment stands in clear contrast to the very different ultrafast kinetics detected between solvents and the protein environment. It is also confirmed by the observation of the vibrational coherences of the torsional mode of retinal, whose frequency was also found

* Corresponding author. E-mail: majed.chergui@epfl.ch; phone: +41 21 6930457.
[†] Sincrotrone Trieste Elettra.
[‡] Institut de Physique et Chimie des Matériaux de Strasbourg.
[§] Ecole Polytechnique Fédérale de Lausanne.

10.1021/jp8077216 CCC: $40.75
Published on Web 02/27/2009

TABLE 1: Solvent Parameters and Steady-state Properties of Absorption and Emission Bands of the All-trans PSBR in Solution

solvent	cHex	DCM	OctOH	MeOH	ACN
ε_r ($\omega = 0$)*	2.02	8.93	9.8	32.66	35.94
n_d	1.424	1.421	1.4295	1.327	1.342
F (ε_r, n_d)	0	0.47	0.49	0.71	0.71
λ (W K^{-1} m^{-1})	0.124	0.148	0.166	0.1977	0.2034
κ (10^{-3} cm^2 s^{-1})	0.86	0.92	0.86	1	1.16
$\bar{\nu}^A$ (cm^{-1})	21485	21290	21880	22350	22015
Γ^A (cm^{-1})	4700	4750	4860	4850	4910
$\bar{\nu}^F$ (cm^{-1})	14450	13890	14050	13850	13830
Γ^F (cm^{-1})	6170	4460	6000	3840	3430
$\Delta\bar{\nu}$ (cm^{-1})	7035	7400	7830	8500	8185
$\Delta\bar{\nu}_{solv}$ (cm^{-1})	0	365	795	1465	1150

* The values in each row are, respectively: static dielectric constant, refractive index, reaction field factor $(\varepsilon_r - 1)/(2\varepsilon_r + 1) - (n_d^2 - 1)/(2n_d^2 + 1)$, thermal conductivity, thermal conduction diffusivity (all at 25 °C, taken from ref 64), band maximum and fwhm of absorption and emission, and the absorption-emission Stokes shift and its intermolecular part (only due to solvation).

to be independent of the solvent,[30] whereas it changes markedly between solvents and protein.[27,31] This lack of sensitivity to the environment and the analysis of the steady-state spectra led us to conclude that the ultrafast processes are mainly intramolecular in nature, and that in the protein, the isomerization dynamics is mainly governed by steric effects.

The isomerization efficiency was previously determined by high-performance liquid chromatography (HPLC) to be <17% in MeOH and hexane,[10−12] or by NMR measurements in DCM.[32] In acetonitrile (ACN), it was found to be larger, ∼27%,[12] although the dielectric constant, viscosity, and heat conductivity of ACN are very close to those of methanol (Table 1). Building on our previous reports,[29,30] we present a complete study of the ultrafast fluorescence of PSBR in various solvents, including ACN, as a function of excitation wavelength. We present a detailed spectral decomposition of the time-resolved emission spectra, which clearly separates the vibrationally cold emission from the S_1 state from higher energy contributions, such as vibrationally hot emission and emission from higher electronic states. The general picture that emerges highlights the conformational heterogeneity of the S_1 surface of retinal in solvents, that is. the existence of up to three independent minima, as evidenced by the multiexponential decay of the vibrationally relaxed fluorescence. We then discuss the possible relation of the various decay channels to the reactive and nonreactive paths that have been reported in solvents.[10−12,32] Notably, these channels are populated differently according to the excitation wavelength and the solvents. Solvents effects show up in acetonitrile as opposed to the other solvents, and they mainly affect the population channel of the different fluorescence channels. Overall, excited-state heterogeneity seems a characteristic feature of PSBR in solvents. This is in stark contrast with the protein for which the isomerization yield is wavelength-independent[33] and where only one quasi-stationary state seems to describe the dynamics.[34,35]

Experimental Methods

The n-butylamine Schiff bases of all-trans retinal were prepared according to previously described methods[26] and protonated using a 3−5-fold excess of trichloracetic (TCA) or trifluoroacetic (TFA) acid. No difference in the acquired data due to the change of the counterion was noticed. The solvents studied are cyclohexane (cHex), dichloromethane (DCM), octanol (OctOH), methanol (MeOH), and acetonitrile (ACN), which differ greatly in their dielectric, thermal, and viscous properties (Table 1).

A 250 kHz regenerative amplifier (Coherent RegA 9050) and a near-IR OPA delivered 40−50 fs pulses at 800, 850, or 1140 nm. All these wavelengths were used for gating the fluorescence in order to cover the complete PSBR fluorescence spectrum (420−950 nm) with the polychromatic fluorescence up-conversion setup, described in detail previously.[29,36−38] Time-resolved fluorescence spectra obtained with different gate wavelengths are corrected for the instrumental spectral response using steady-state spectra and then merged together. The setup has time and spectral resolution of 100−125 fs and 14 nm, respectively. In both the steady-state and the time-resolved experiments, excitation was at either 400 or 570 nm on the blue or red wing of the absorption band (arrows, Figure 1), respectively. Care was taken to work in the linear regime of excitation powers. The sample was recirculated in a flow cell, at a speed ensuring its renewal between shots. Also, only <20% of the molecules were excited per laser shot, such that accumulation of cis-isomers remained under 10% in a typical scan of 1 h duration.

Steady-state absorption spectra are recorded in a Perkin-Elmer (Wellesley, MA) or Shimadzu spectrophotometer. Steady-state fluorescence was measured using either a modified Spex (Edison, NJ) fluorimeter, a fiber fluorimeter (Ocean optics, FL), or the same CCD camera and spectrometer as in the up-conversion setup. The fluorescence spectra $\mathrm{Fl}(\lambda)d\lambda$ are corrected for the instrument response, determined by using standard red-emitting dyes, and multiplied by λ^2 upon conversion from wavelengths to wavenumbers.[39] The steady-state fluorescence spectra are obtained on samples with optical density 0.5−0.6/cm under excitation at 400 nm or 0.05−0.07/cm at 570 nm.

The kinetic traces are fitted to analytical convolution of a sum of exponentials multiplied by the unit step-function and a Gaussian whose width is equal to our time resolution. One rise exponential (decay constant $\tau_{rise;}$ amplitude $a_{rise} < 0$), and up to three decay exponentials (τ_1, τ_2, and $\tau_{3;}$ a_1, a_2, and $a_3 > 0$) suffice to successfully describe our data. The ratio of $a_{rise}/\sum a_i$ (which must be <1 since the fluorescence signals are only positive) gives us the percentage of the rise having a τ_{rise} constant, and the rest of the signal is assumed to appear with a rising constant much smaller than our best time resolution of 100 fs.

Results

Steady-state Spectra. In our previous report,[29] we presented steady-state absorption $\mathrm{Ab}(\bar{\nu})$ and emission spectra $\mathrm{Fl}(\bar{\nu})$ of PSBR in MeOH, OctOH, and cHex with the carboxylate anion of TCA as counterion. Figure 1 shows the absorption $\mathrm{Ab}(\bar{\nu})/\bar{\nu}$, and emission $\mathrm{Fl}(\bar{\nu})/\bar{\nu}^3$ line shapes, since they reflect the transition

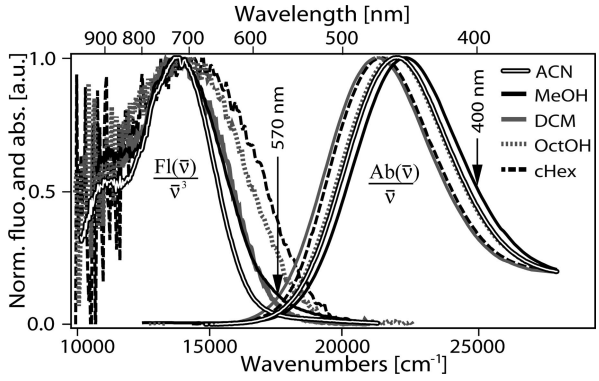

Figure 1. Steady-state absorption and fluorescence lineshapes of all-trans PSBR in ACN, MeOH, DCM, OctOH, and cHex excited at 400 nm (right arrow). 570 nm excitation (left arrow) was also used for the measurements shown in Figures 2−5.

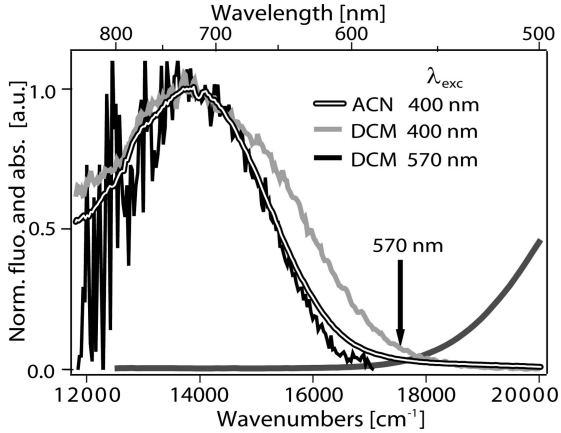

Figure 2. Steady-state fluorescence lineshapes of PSBR in ACN upon 400 nm excitation, and in DCM upon 400 and 570 nm excitation. The blue-most curve (dark gray) is the steady-state absorption of PSBR in DCM.

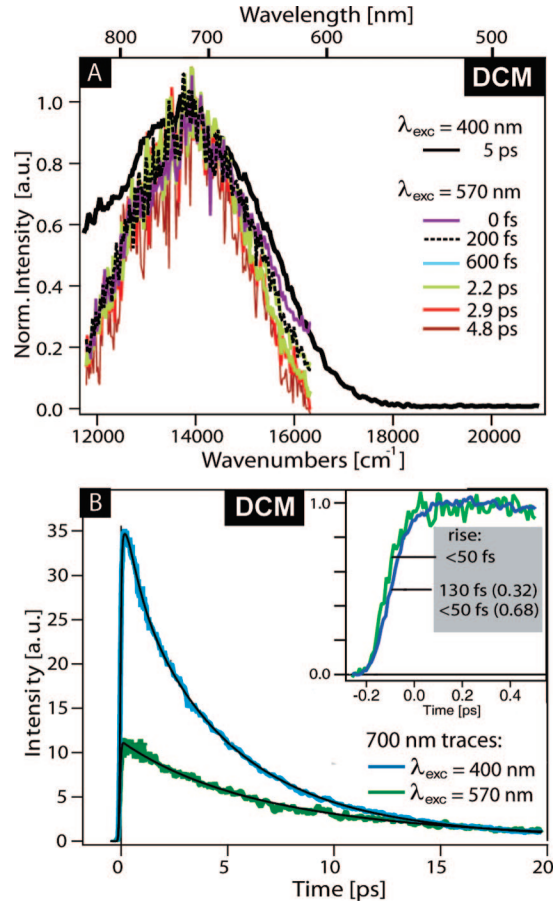

Figure 3. (A) Normalized fluorescence lineshapes of the all-trans PSBR in DCM at different delays (0−4.8 ps) obtained upon 570 nm excitation, and for $t = 5$ ps upon 400 nm excitation. (B) Fluorescence decay curves of the emission of PSBR/DCM at 700 nm obtained upon 570 (green line) or 400 nm excitation (blue line). Note the traces obtained from the biexponential decay and biexponential rise/triexponential decay fit (black lines, see rise and decay constants in Table 2 for the a-band). The inset zooms into the first 0.6 ps of the traces and gives the rise times obtained from the multiexponential fit. The residuals of the fits are given in the Supporting Information section.

probability.[40,41] In addition to the above solvents, Figure 1 includes spectra in the non protic DCM and ACN solvents. Table 1 lists the band maxima and widths of the steady-state absorption and emission bands, as well as the absorption-emission Stokes shifts ($\Delta\bar{\nu} = \bar{\nu}^{A} - \bar{\nu}^{F}$). The former are obtained by fitting the bands with the skewed Gaussian function that describes well the broad asymmetrical spectra of retinal proteins.[42−45]

If we consider the shifts with respect to cHex, which is the least polar of all solvents, for protic solvents and ACN we find that the absorption band shifts to the blue (Table 1), whereas in DCM it shifts slightly to the red (hypsochromic shift). These shifts are overall small (at most ∼900 cm^{-1}), as previously reported,[11,46,47] especially in view of the large differences in dielectric constants (cf. Table 1) and a difference dipole moment $\Delta\mu = 12$ D.[14] A clue for understanding this discrepancy may lie in the fact that the system consists of two dipoles: the Schiff base cation−counterion dipole and the dipole made up by the charges on the conjugated backbone of retinal Schiff base. The former actually involves a hydrogen bond N(δ^+)−H−COO(δ^-), as can be seen from the effect of fluorinated alcohols on the absorption spectrum.[48] Increasing solvent polarity stabilizes the N(δ^+)−H−COO(δ^-) ground state. The N(δ^+)−H−COO(δ^-) dipole is reduced in the excited state, as photoinduced charge translocation on the retinal backbone effectively decreases the N(δ^+) charge. This would lead to a strong hypsochromic shift for this hydrogen-bonded dipole. Regarding the conjugated charges on retinal, a dipole moment increase is expected to yield a bathochromic shift. Both effects almost cancel each other, although a slight hypsochromic shift is still observed. One has to keep in mind, however, that other factors (e.g., homoconjugation of TCA and TFA[48]) also strongly affect the position of the absorption maximum.

As discussed in refs 29, 47, and 49 the absorption-emission shift in apolar cHex represents the intramolecular contribution to the total Stokes shift. Relative to the latter, the absorption−emission Stokes shifts ($\Delta\bar{\nu}$) are slightly larger in the other solvents (at most ∼1500 cm^{-1}), and a strong change of the fluorescence spectral width is observed (Table 1). As already reported,[29] the intermolecular contribution to $\Delta\bar{\nu}_{solv}$ is very small (see below).

Note that the observed Stokes shifts have to be interpreted with caution. As a matter of fact and in contrast to dye molecules with longer fluorescence lifetimes, the time-integrated spectral properties of the PSBR cation are the result of a more subtle interplay of electronic relaxation, vibrational relaxation, and solvation dynamics, acting on the same time scale as the average excited-state lifetime of 3−4 ps.[29,50,51] The importance and time scale of vibrational relaxation can be qualitatively evaluated by comparing the effect of different excitation wavelengths. When exciting at 570 nm, near the energy at which the absorption

TABLE 2: Results of the Data Analysis for the Time-resolved Fluorescence of the All-trans PSBR in Solution*

solvent	cHex	DCM	OctOH	MeOH	ACN
400 nm Excitation					
a-band:					
τ_{rise1}/fs	<30 (0.66)	<30 (0.68)	<30 (0.60)	<30 (0.45)	<30 (0.58)
τ_{rise2}/fs	80 (0.34)	130 (0.32)	130 (0.40)	110 (0.55)	190 (0.42)
τ_1/ps	1.3 (0.7)	0.6 (0.25)	1.1 (0.43)	0.9 (0.22)	
τ_2/ps	3.4 (0.3)	4.2 (0.62)	4.2 (0.57)	4.0 (0.72)	4.0 (0.28)
τ_3/ps		11 (0.12)		13 (0.06)	8.4 (0.72)
$\langle\tau\rangle$/ps	1.9	4.1	2.9	3.9	7
$\Phi_1 \times 10^{-4}$	0.85			0.18	1.02
$\Phi_2 \times 10^{-4}$	0.95			2.61	5.48
$\Phi_3 \times 10^{-4}$				0.71	
$k_1 \times 10^{11}$	7.7	1.7	9.1	11.1	7.7
$k_1 \times 10^{11}$	2.9	2.4	2.4	2.5	2.9
$k_1 \times 10^{11}$		9.1		0.8	
b-band:					
τ_b/ps	1.2	1.7		2	0.48
c-band:					
τ_c/ps	0.21	0.47		0.44	0.35
570 nm Excitation					
a-band:					
τ_2/ps		4.2 (0.38)			
τ_3/ps		11 (0.62)			

* The values in each row are: rise and decay time constants τ_i; relative amplitudes (in parentheses) of the ith channel of a-band; $\langle\tau\rangle$, average decay time of the a-band defined as $\sum_i^3 a_i\tau_i$; Φ_i, fluorescence quantum yield (see the Supporting Information section); and k_i, rate of the ith channel of a-band; decay time constants τ_b and τ_c for b- and c-band. Lifetimes are given with the following uncertainties: $\tau_{rise1} \pm 20$ fs, $\tau_{rise2} \pm 50$ fs, $\tau_{1,2} \pm 0.5$ fs, $\tau_3 \pm 3$ ps, $\tau_b \pm 0.3$ ps, and $\tau_c \pm 0.08$ ps.

and emission spectra intersect, in principle no or little excess energy is delivered to the chromophore that could populate higher vibrational states in the excited state. We therefore refer to this situation as the "equilibrated spectra". In addition, according to the two-photon thermal lensing study by Birge et al.,[52] at 570 nm only one-photon transitions (exclusively S_0-S_1 at these energies) can be excited. On the other hand, at 400 nm also the S_2 state may be accessed, although the S_0-S_2 transition is unresolved in the absorption profile, as it has mixed one- and two-photon transition character.[52]

Figure 2 compares the steady-state fluorescence spectra of PSBR in ACN excited at 400 nm and in DCM excited at 570 and 400 nm. In the latter case the fluorescence is broadened on the high energy side, whereas under 400 nm excitation the spectrum in ACN approaches the equilibrated spectrum, necessary for the evaluation of the Stokes shift (see below). We note that the fluorescence width Γ^F depends on the solvent and seems to decrease with increasing thermal conductivity and diffusivity of the solvent (Table 1). Upon 400 nm excitation, the chromophore receives an excess energy of $\Delta\nu_{excess} > 6000$ cm^{-1} with respect to the 0−0 energy of the S_0-S_1 transition. On the basis of the above, it makes sense to attribute part of the blue wing observed upon 400 nm excitation to vibrationally hot contributions, and/or to higher electronic states. However, in ACN the fluorescence upon 400 nm excitation is almost identical in profile to the fluorescence in DCM upon 570 nm excitation, which suggests a dramatically efficient electronic and vibrational relaxation process in the former solvent, as confirmed by the time-resolved results presented below.

One last point about the steady-state data concerns the dielectric contributions to the total Stokes shifts. We used the dielectric spherical cavity model of Lippert-Mataga[53−55] to estimate the contribution due to the solvent orientational polarizability. Taking a difference dipole moment $\Delta\mu = 12$ D determined in a *p*-dioxane solvent,[14] and a cavity radius $a = 4.3$ Å, we find a theoretical value of 5500 cm^{-1} red-shift for ACN, that is, 5 times larger than the observed one (1150 cm^{-1}, Table 1). We believe that the steady-state spectrum captures an almost equilibrated situation, as needed for comparison with the model, since in ACN solvation should be terminated in less than 0.63 ps,[56] that is, 5 times faster than the average fluorescence lifetime, and vibrational relaxation is close to being complete (see above). It is possible that the Lippert-Mataga solvation sphere does not account properly for the elongated geometry of retinal, but such a correction is unlikely to account for the large discrepancies we find. Again, a quantitative description of the solvation should rather account for photoinduced modifications of the hydrogen-bonded ion pair and for the dipole moment reversal on retinal, but this is out of the scope of the present work.

In summary, (a) in DCM, a blue wing appears upon 400 nm excitation but not under 570 nm excitation; (b) this blue wing is present in most other solvents (except ACN) at 400 nm; (c) in ACN at 400 nm excitation, the fluorescence is very similar to the 570 nm excited (vibronically relaxed) S_1 fluorescence in the other solvents; and (d) dielectric solvation seems to play a minor role in the overall relaxation of the PSBR chromophore, which is dominated by intramolecular processes.

Time-resolved Fluorescence Spectra. More insight into the relaxation processes is gained from the ultrafast fluorescence measurements upon 570 and 400 nm excitation of PSBR.

a. Identification of Vibrationally Cold Fluorescence. As explained above, excitation at 570 nm leads to vibrationally cold fluorescence. We focus on the DCM solvent, because PSBR in this solvent has a larger optical density at 570 nm (Figure 1), allowing us to perform the time-resolved experiment with satisfactory signal-to-noise ratio. Figure 3A shows the fluorescence recorded at different time delays up to ~5 ps at 570 nm excitation, which we compare to the fluorescence spectrum upon 400 nm excitation, recorded at a time delay of 5 ps, that is, when the system has largely relaxed. The spectral evolution with time of the fluorescence for 570 nm excitation is practically nonexistent, and the spectra for $t < 300$ fs show only a slight broadening at the blue wing. Although, the fluorescence band

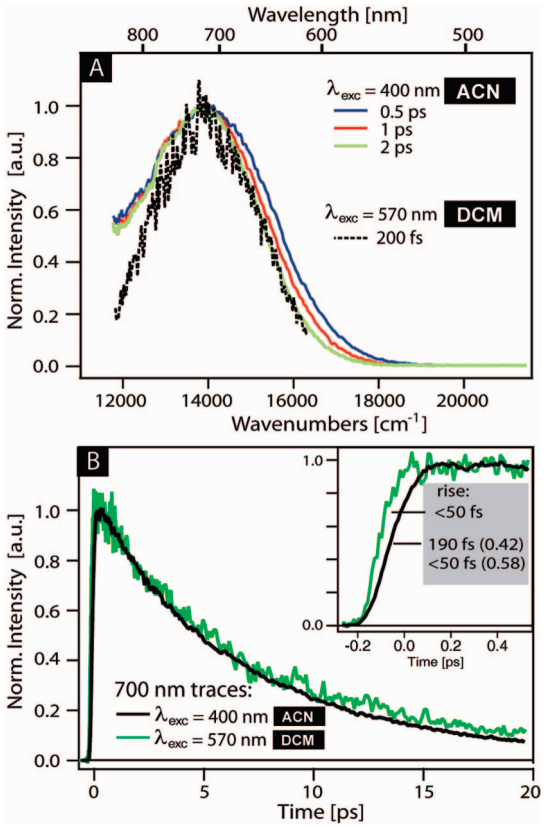

Figure 4. (A) Normalized fluorescence lineshapes of the all-trans PSBR in ACN for 0.5, 1, and 2 ps time delays, upon 400 nm excitation (solid lines) and in DCM for $t = 200$ fs upon 570 nm excitation (dotted line). (B) Fluorescence kinetic traces recorded at 700 nm in ACN upon 400 nm excitation (black line) and in DCM upon 570 nm excitation (green line). The inset zooms into the first 0.6 ps of the traces and gives the rise times obtained from the multiexponential fit.

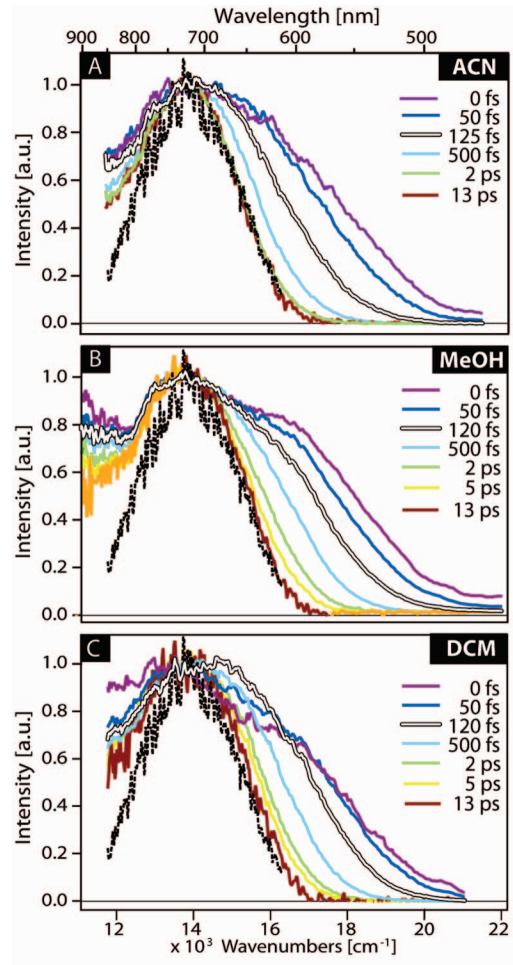

Figure 5. Normalized fluorescence lineshapes of the all-trans PSBR in ACN (A), MeOH (B), and DCM (C) at different times upon 400 nm excitation. The line shape of the same chromophore in DCM at 200 fs upon 570 nm excitation is depicted with dotted lines.

at long time delays (i.e., cold) upon 400 nm excitation, is slightly larger than the 570 nm excited one, the bands agree in position and profile (similar weak asymmetry) in both cases. These last two observations show that we are dealing with a stationary spectral component under 570 nm excitation and under 400 nm excitation for sufficiently long delay times. The lack of spectral shift also confirms that electronic solvation processes are negligible.

Figure 3B shows the kinetic trace recorded at the maximum of the fluorescence (700 nm) upon 570 nm excitation. It can best be fitted by an instrument-limited risetime (≤50 fs) followed by a biexponential decay with time constants of $\tau_1 = 4.2$ ps and $\tau_2 = 11$ ps, and preexponential factors given in Table 2. Because we noted from the steady-state fluorescence (Figure 2) that PSBR/ACN at 400 nm excitation behaves very much like PSBR/DCM at 570 nm excitation, we also compare in Figure 4A the fluorescence of the former for time delays >0.5 ps, with that of the latter at 200 fs time delay (dotted line). At 2 ps delay, the spectra look very similar, which confirms that even under 400 nm excitation, the PSBR fluorescence in ACN is largely cold on a very short time scale. Figure 4B compares their kinetic traces measured at band maximum, showing remarkable agreement, so that the decay times are the same in either solvent, and therefore, the decay channels are identical. The origin of the two decay times in the kinetic traces will be discussed later, but at this stage the above results clearly identify the vibrationally cold fluorescence and provide a very important input to disentangle the additional contributions that appear upon 400 nm excitation. In addition, they also clearly point to a heterogeneous S_1 surface in the sense that more than one emitting species stems from it. The inset in Figure 4B zooms into the rising part of the kinetic traces and shows that although the rise is prompt at 570 nm excitation in DCM, it has an additional longer component (∼200 fs) in ACN at 400 nm.

b. 400 nm Excitation. When excited at 400 nm, the PSBR fluorescence spans a large spectral range between 440 and 900 nm, as can be seen in Figure 5. In all solvents, the early emission spectra ($t < 100$ fs) cover a spectral range of about 500 nm, with a maximum around 720 nm. The evolution of the maximum and fwhm in time is conveniently followed by the time-dependence of the first and the second spectral moments (M_1 and M_2, respectively) that are shown in Figure 6 for MeOH. Note that the moments are calculated for the emission in our experimental window ranging from 450 to 920 nm, although the PSBR fluorescence extends even more to the red. Both M_1 and M_2 can best be fitted using triexponential functions having similar decay constants of ∼80 fs, ∼700 fs, and >14 ps. The uncertainty on the latter is very large (∼15 ps) since our scans cover a range of 20 ps and the fluorescence lifetime is limited to 3−4 ps.

In all solvents, the high-energy side decays rapidly ($\tau_1 \approx 80$ fs), causing spectral narrowing and shift of the maximum to lower energies; by $t = 100$ fs, the spectrum has narrowed by 1000 cm^{-1} in MeOH and DCM and by 1700 cm^{-1} in ACN (Figure 5, double line). In the second phase ($t > 100$ fs),

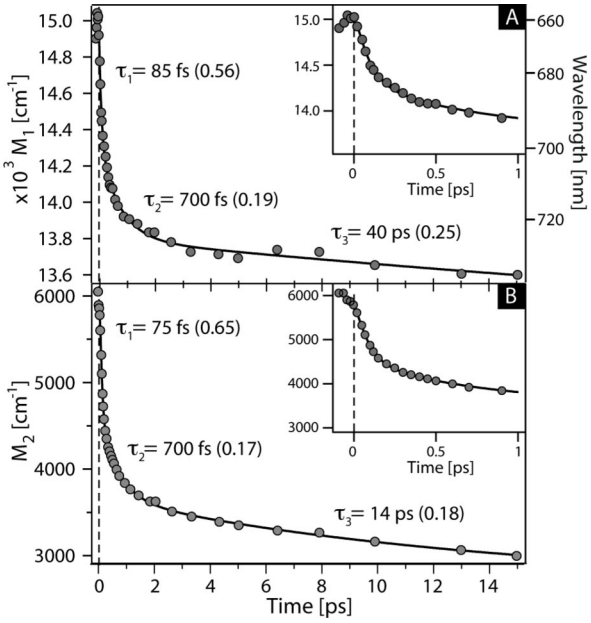

Figure 6. First (A) and second (B) spectral moments of fluorescence of the all-trans PSBR in MeOH. Decay constants τ_i and relative amplitudes (in parentheses) of the *i*th decay are given. The inset zooms into the first picosecond of the moments. Decay constants are given with the following uncertainties: $M_1 - \tau_1 \pm 20$ fs, $\tau_2 \pm 200$ fs, $\tau_3 \pm 25$ ps; $M_2 - \tau_1 \pm 10$ fs, $\tau_2 \pm 100$ fs, $\tau_3 \pm 7$ ps. The residuals of the fits are given in the Supporting Information section.

significant narrowing occurs most prominently on the high-energy part on a time scale of $\tau_2 \approx 700$ fs, which causes a gradual red-shift of M_1 at $t = 2$ ps, and it reaches the final value close to 720 nm in all studied solvents. For time delays larger than 2 ps, maximum and width of the fluorescence of PSBR in ACN remain constant, and the fluorescence spectrum coincides with the vibrationally relaxed fluorescence of PSBR in DCM (dotted line, Figure 5A). In contrast, in MeOH and DCM, band narrowing continues with a slow time constant ($\tau_3 > 14$ ps) eventually converging to the vibrationally cold fluorescence (dotted lines, Figure 5, panels B and C). In conclusion, the origin of the spectral maximum shift in all solvents is primarily due to narrowing of the fluorescence on the high-energy side, stressing once more the lack of noticeable dielectric solvation shift.

Figure 3B shows the kinetic trace of PSBR in DCM at 700 nm, upon 400 nm excitation. We fitted it by a biexponential rising component followed by a triexponential decay, and the fit parameters are given in Table 2. Since it is recorded at the same wavelength as the curve at 570 nm excitation (same figure), we retained the decay constants extracted from this curve, while their preexponential factors were left free. The quality of the fit is excellent with an additional rising component of 130 fs and an additional decay component of $\tau_1 = 0.6$ ps. Note that the ratio of preexponential factors of the second and third component are very different to those extracted from the fit of the decay curve at 570 nm excitation (Table 2). This suggests that the decay channels responsible for these components are populated differently at 400 and 570 nm.

c. Spectral Decomposition. To disentangle the different spectro-temporal components that make up the fluorescence spectra at different time delays, we have proceeded by stepwise subtraction of spectral components. Figure 7 shows the case of PSBR/MeOH. Because, in all solvents, the equilibrated fluorescence band (Figures 3 and 4) lives significantly longer than the other spectral features, it represents a particular spectro-temporal component (Figure 7B). If there is a wavelength range where only this band contributes, then the normalized transients are constant in time. This behavior is indeed found for almost all solvents and within 50 nm red or blue of the band maximum (690−730 nm). This spectral region defines the so-called a-band that is then subtracted from the entire 2D data, leaving the residual spectra shown in Figure 7C. They consist of a broad band fixed at 12 000 cm^{-1} for all time delays, and another stronger one that evolves spectrally in the region of 16 000−18 000 cm^{-1}, but only at early times. Indeed, normalizing the spectra obtained for time delays ≥2 ps (Figure 7D) thus identifies an additional nonshifting component (b-bands), which we assume to be spectrally invariant for shorter times as well. The transients of the 12 000 cm^{-1} signal in Figure 7C allow us to trace the time-dependent amplitudes of the b-bands shown in Figure 8B, 8D and 8F (red lines). They turn out to be a sharply rising monoexponential with a decay constant of ∼2 ps in MeOH and DCM and ∼0.5 ps in ACN. We then subtracted the b-bands with the proper decay from the residual spectra at all time delays and recover a last component (the c-band) that exhibits spectral evolution. Finally, Figure 8 confronts the a-, b-, and c-bands and their associated kinetic traces for PSBR in ACN, MeOH, and DCM.

Interestingly, the b-bands do not exhibit the same intensity in all three solvents. Relative to the a-band, they are more intense in MeOH than in ACN or DCM, and this is not reflected in the decay times. The evolving c-band is weakest in ACN but shows very similar behavior in all solvents (Figure 8, panels A, C, and E, spectra in blue tones). The dynamic red-shift is due to a high-energy wing ($\lambda < 550$ nm) decaying predominantly within our time resolution, but a less-intense 235 fs decay component is also present.[29] The latter is most probably not related to the rise of the a-band, since it remains constant in every solvent whereas the τ_{rise2} constant of the a-band increases in going from cHex to ACN (Table 2). For $\lambda > 580$ nm, the c-band decays monoexponentially with a 350−440 fs time constant (Figure 8, panels B, D, and F, blue traces). The decay of c-band is determined from the transients of the signal at 590 nm, that is, at the average value of the maxima for different time delays (blue lines, Figure 8, panels B, D, and F).

The fit parameters of the kinetic traces of the three components are given in Table 2. Interestingly, as already implicit from Figure 4B, we confirm that the shortest decay component τ_1 is missing in ACN. In contrast, the rise remains unresolved for the b-band, which also exhibits the fastest decay time in ACN.

Discussion

The above results clearly identify three spectral components and up to five characteristic time scales, which show some solvent- and excitation energy-dependence. We now discuss their origin and the way they characterize the dynamics in solution as opposed to the protein.

Origin of the Spectral Features. The a-band is clearly a vibrationally relaxed fluorescence in all the solvents studied and is the lowest lying in energy. It represents transitions from the $\nu = 0$ vibrational level of S_1 to the vibrational levels of the ground state ($\nu^* = 0 \rightarrow \nu = 0, 1, 2...$) and spans several quanta of the C=C stretch vibrations (1562 cm^{-1}, ref 57).

As both the b- and c-bands do not show up under low-energy excitation, we conclude that they are related to higher vibrational and, possibly, electronic states. Concerning the b-bands, their doublet structure suggests a vibrationally hot emission, although it is not clear from which level it stems. If we consider the

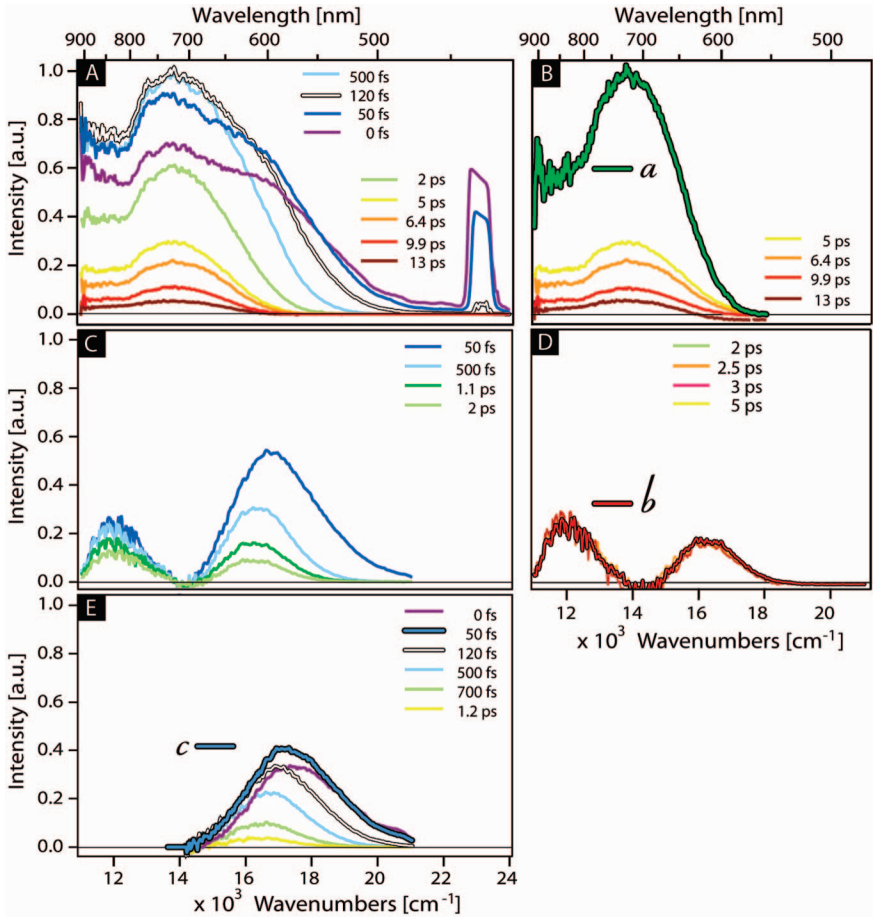

Figure 7. Spectral decomposition procedure of the fluorescence (see text for details). (A) Raw data of the PSBR fluorescence in MeOH; (B) a-band (green line) obtained by averaging spectra for $t \geq 5$ ps (yellow to dark red lines) and normalized to maximum intensity; (C) Residual spectra after subtraction of the a-band for $t \leq 2$ ps; (D) as in panel C but spectra are normalized for $t \geq 2$ ps; the b-band (dark red line) is normalized to maximum intensity; (E) residual spectra after subtraction of the b-band; the c-band (blue line) is represented by the spectrum at maximum intensity.

C═C stretch modes, with an adiabatic transition energy of ~18 000 cm^{-1} (difference between the energy at absorption maximum minus the half-width at half-maximum) for all solvents, we find that 400 nm excites high lying vibrational levels around $\nu = 4$. With our 50 fs excitation pulse (spectral width $\approx$ 670 cm^{-1}), we can excite stationary levels of the high frequency modes. This should give rise to a short-lived vibrationally hot emission with a progression having an intensity pattern with more than one maximum. We refrain from a simulation of the intensity pattern, since we do not know precisely which modes are excited, nor their relative weights in the emission spectrum and relaxation efficiencies. It is sufficient to note that the doublet structure of the b-band is strong evidence of a vibrationally hot emission, which we assign to modes having frequencies typically above 700 cm^{-1}.[57,58]

The spectral evolution (red shift and narrowing) of the c-band points to a wave packet motion sliding down a potential slope. It is clearly not due to solvation, as it is also observed in the less polar DCM, for which the 570 nm excitation shows no spectral evolution (Figure 3A). As 400 nm excitation may also reach the S_2 state, which for the retinal cation in solvents approaches S_1 and is even intertwined to it along part of the isomerization coordinate,[59,60] the c-band could possibly come from the S_2-S_0 emission, which has sizable oscillator strength due to mixing with S_1. As the 300−400 fs decay of the c-band does not show up in the rise of the other bands, we conclude that the S_2 state is not connected to S_1 (Figure 9) and that its spectral evolution reflects its relaxation, due to cooling.

Fluorescence Decay Channels. Although the spectroscopic data shows that the a-band is clearly a vibrationally relaxed emission, its decay kinetics exhibit three channels, with typical lifetimes of 0.6−1.3, 3−4, and 8−13 ps, hereafter denoted I−III, respectively. This in itself shows that the S_1 fluorescence stems from a complex hypersurface, with probably three minima, each corresponding to a radiative decay channel, in addition to the hot fluorescence giving rise to the b-bands. This hypersurface must be shallow in the region of the minima since the emitting channels cannot be spectroscopically distinguished. Also, the population in the different minima are not in equilibrium, that is, population exchange is very slow, as they seem to decay independent of each other.

If we then consider the a-band under low energy excitation (570 nm) in DCM and 400 nm in ACN, we find that it contains only channels II and III, with the latter being dominant. In ACN, the risetime has an additional 190 fs component, although it is prompt (≤50 fs) in DCM under 570 nm excitation. These two components are recovered under 400 nm excitation, in the other solvents, but this time channel III is a minor contribution to the point that it disappears in some solvents. The similarity in spectral profile of the a-band under these different conditions (Figure 4) suggests that the biexponential decay corresponds to two different minima in the S_1 potential surface, with preexponential factors reflecting the relative population of these channels. It is obvious that the branching of population to channels II and III is similar in DCM at 570 nm excitation and in ACN at 400 nm excitation, although the time it takes to

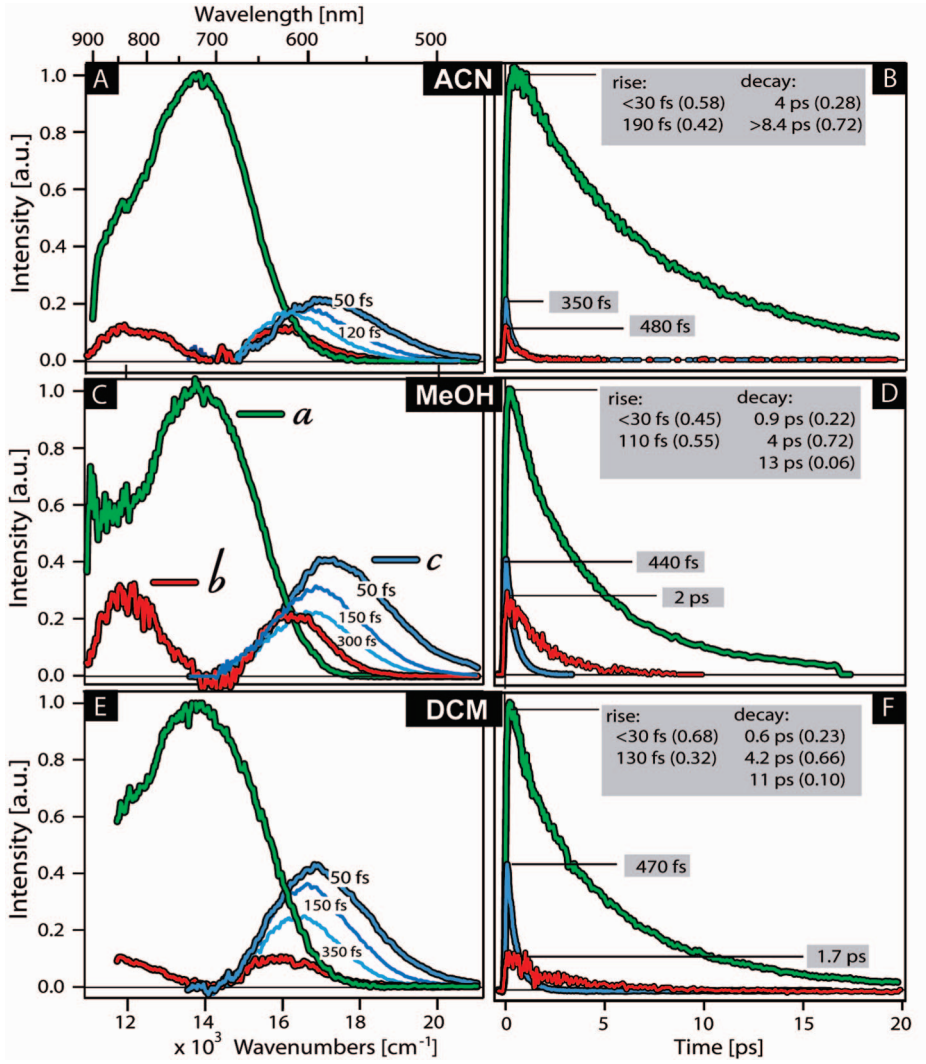

Figure 8. Decay-associated spectra-DAS (A, C, E) and their corresponding kinetic traces (B, D, E) recovered from the spectral decomposition analysis of all-trans PSBR in ACN, MeOH, and DCM excited at 400 nm: a-band, b-band, c-band. The spectra are plotted for a delay time corresponding to their maximum intensity. For the c-band, two additional spectra at the delay times belonging to the 120−150 and 200−350 fs ranges were added (dark and light blue, respectively). The rise and decay constants with their relative amplitude (in parenthesis) are given in a text box placed near each time trace. The residuals of the fits are given in the Supporting Information section.

populate them is not identical. However, upon 400 nm excitation in the other solvents, channel I is also populated, whereas channel III is unfavorably populated in this case. Also, we find that channel II is dominant in alcohols (and in DCM), but its weight decreases in going from light to heavy ones, and it is a minor channel in cyclo-hexane. All these decay channels then evolve independent of each other. The general picture that emerges is that not only does the S_1 fluorescence stem from several minima, but the population pathways to these radiative channels differ with the excitation energy and with the solvent.

It is tempting to relate the decay channels to the photoproducts found by HPLC, keeping in mind that the latter have been determined under steady-state conditions (i.e., infinite times), while our measurements capture decay channels within picoseconds and do not include further conformational changes after the system has gone back to the ground-state surface. In this respect, cHex can be expected to be similar to n-hexane, which is known to have the lowest isomerization efficiency of all solvents.[10−12] cHex shows the largest contribution of channel I, and we would thus attribute the latter to the return to the initial state, that is, repopulation of all-trans S_0, which we call a nonreactive pathway hereafter. Consistent with ACN having the highest isomerization yield,[12] we find that the putative nonreactive channel I is lacking in ACN, as only channels II and III are observed.

The slower decay channels II and III would then be attributed to isomerization (reactive pathways) to the 11-cis and the 9-cis forms, in conformity with previous assignments.[26,61,62] The nonreactive channel I is expected to win over the reactive ones, as the isomerization efficiency is low in solvents (15−20%). Channels II and III lead to conical intersections, where additional trans−cis partition takes place, which may be the main effect limiting the isomerization yield of ACN (27%) and the other solvents.

An alternative explanation for multiexponential decay behavior has been proposed in the literature. The influence of small barriers on the decay kinetics of the excited-state surface was investigated computationally by Olivucci and co-workers.[63] They showed that the barrier induces multiexponential decays even when one single minimum is present separated from the conical intersection by a shallow barrier. Multiexponentiality is then related to different amounts of kinetic energy in the reactive torsional mode, with the faster decay time reflecting molecules that possess enough kinetic energy to overcome the barrier at a

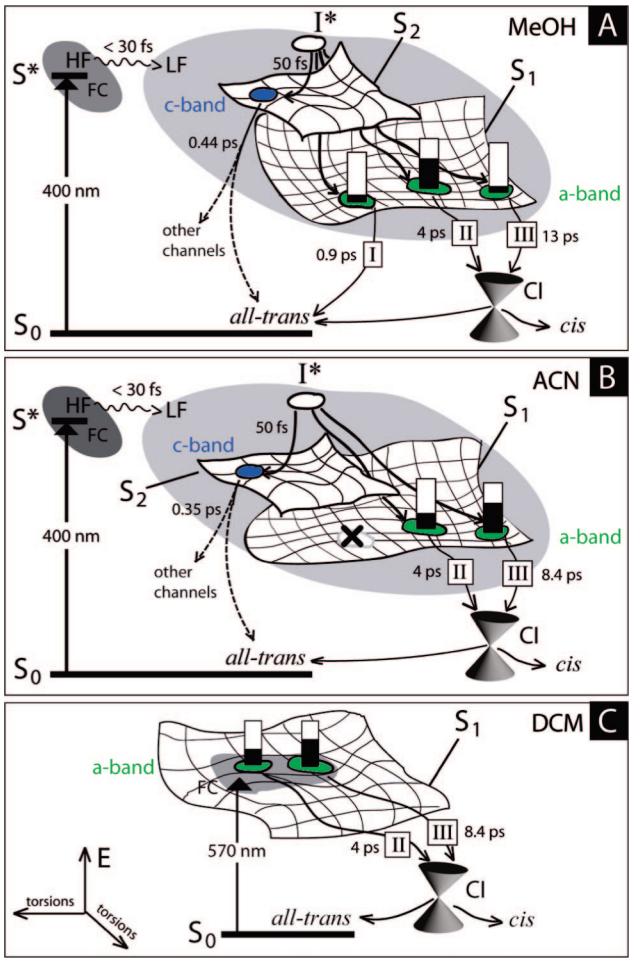

Figure 9. Schematic representation of the channels to the stationary points (SP, black lines) on the S_1 and S_2 surfaces for PSBR in: (A) MeOH, (B) ACN upon 400 nm excitation and, (C) DCM upon 570 nm excitation. The blue shaded areas represent the SP of the c-band. The bar graphs reflect population in the SPs of the a-band (green shaded areas) at $t = 150$ fs. [A completely filled bar graph corresponds to the population that would give the intensity of DAS equal to 1, in units used in Figure 8, panels A, C, and E. The populations were calculated by multiplying the DAS intensities obtained from Figure 8, panels A, C, and E, by the decay amplitudes from Table 2. (e.g., at $t = 0$, a2 population for PSBR in MeOH is I(a-band, $t = 0$) · Amp(a-band, $\tau 2$) $= 0.6 \times 0.72) = 0.4$.]

higher rate. It was found that PSBR in MeOH has a 600 cm^{-1} barrier along the reaction coordinate.[62] In our work, the decay time of the b-band indicates that vibrational relaxation occurs on a 1.5−2 ps time scale (in all solvents but ACN), only a factor of 2 shorter than channel II. It is thus possible that channels II and III be related to the same S_1 minimum, but reflect the spreading in kinetic torsional energies around this same minimum. As the 570 nm excitation in DCM leaves the molecules with less excess energy, the kinetic energy argument can explain the increasing amplitude of channel III observed in this case. However, this explanation does not seem to bind together all of our observations, as we will see in the next section.

Relaxation Pathways. The relaxation pathways leading to the different excited-state minima show some solvent dependence, as can be seen from the preexponential factors, with ACN (maybe also cHex) clearly standing out of the trends in the other solvents.

Along the theoretical model by Gonzalez-Luque et al.,[64] but extended to a situation of up to three "stationary fluorescent points" on the S_1 hypersurface, we propose the following scenario for the relaxation leading to the radiative decay channels. The ultrafast rise of ≤30 fs is most probably the relaxation along high-frequency skeletal modes, overdamped by anharmonic coupling to low-frequency modes,[30] and it is the first event associated with bond order change in S_1 (wavy arrow, Figure 9). Loosening of the C═C bonds leads to the population of various local minima on the excited-state surfaces, as movements along different torsional coordinates become more probable. In line with the above, we therefore propose that the emission of the a-band stems from several local minima (called stationary points, SP[64]) on the S_1 potential surface, respectively, corresponding to different torsional conformations of the chromophore and giving rise to the different decay times observed. In addition, vibrational levels with frequencies above 700 cm^{-1} are excited, which additionally give rise to the b-bands. Figure 9 depicts schematically the above scenario. Ultrafast (<30 fs) relaxation from the FC excited region into a nonstationary point on the excited-state surfaces which we label **I*** is the primary event. Further relaxation leads to population of the SPs on the S_1 surface belonging to the a-band (green shaded area, Figure 9) and of a SP on the S_2 surface giving rise to the c-band (blue shaded area, Figure 9).

One of the most outstanding features of the present work is the very fast energy relaxation in ACN, which shows, upon 400 nm excitation, the same decay channels as observed under 570 nm excitation in DCM, since the decay times are identical in both solvents (Figure 4B). Clearly, the difference with other solvents lies in the way channels I−III are populated. We believe that ACN may affect the hypersurface on which the dynamics runs in such a way that channel I is missed, and channels II and III are differently populated than in the other solvents (Table 2). An alternative explanation would be that the solvent affects the structure of the PES of S_1, such that the minimum associated to channel I is nonexistent, and those related to channels II and III are different. That the environment has a strong influence on the PES is already obvious from the comparison of solvents and the protein environment.[29] The steric conditions are obviously different in the protein, but so is the electrostatic environment, as can readily be seen from the red-shifted peak of the absorption spectrum in the protein. The action of ACN is more difficult to understand: although it dissipates more favorably the excess energy needed to relax down to the S_1 surface, at the same time either modifying the pathways to the different minima on this surface or canceling one of them (channel I in this case), it is known to slow down relaxation compared to water in other cases,[65] but it is also characterized by an outstanding inertial solvation dynamics.[56] As the different solvent polarities and hydrogen-bonding abilities of solvents other than ACN do not influence the reaction speed, one may suggest that the Schiff base cation−counterion properties are more important. This needs to be checked in future work. More, possibly, theoretical work is needed to explain the behavior in ACN, which besides accelerating vibrational relaxation seems to affect the excited-state potential of the protonated retinal Schiff base.

Conclusions

In this article, we presented a study of the solvent effects on the ultrafast relaxation kinetics of protonated Schiff bases of retinal in both protic and aprotic solvents, using femtosecond fluorescence up-conversion techniques with broadband detection at two excitation wavelengths (400 and 570 nm). In all solvents, the system exhibits multiple (three, except ACN that has two)

emitting species, which we identify as emissions from different isomers on the relaxed S_1 surface, in addition to vibrationally hot S_1 fluorescence and emission from the S_2 state, which shows spectral evolution on the time scale of 300−400 fs. The emitting species of the relaxed S_1 state were kinetically, rather than spectroscopically, distinguished and point to its heterogeneity (several energetically close-lying minima). The remarkable feature of all emissive species (relaxed and unrelaxed) is their weak (or lack of) solvent dependence. Acetonitrile stands out as a solvent in that its emission spectrum at 400 nm excitation is similar to the 570 nm excited (i.e., with no excess vibrational energy) S_1 fluorescence in DCM. Incorporating ACN in the present data set, which has the highest isomerization yield, allows us to give a stronger support to our previously suggested assignment[29] of the ≈1 ps decay components being a dominantly nonreactive excited-state path. Finally, these results reinforce our previous conclusion that in the protein, the steric effects and/or the distribution of the (inhomogeneous) local electric field determine the high yield of isomerization.

Supporting Information Available: This material is available free of charge via the Internet at http://pubs.acs.org.

References and Notes

(1) Oesterhelt, D.; Stoecken, W. *Nature—New Biology* **1971**, *233*, 149.
(2) Dexheimer, S. L.; Wang, Q.; Peteanu, L. A.; Pollard, W. T.; Mathies, R. A.; Shank, C. V. *Chem. Phys. Lett.* **1992**, *188*, 61.
(3) Dobler, J.; Zinth, W.; Kaiser, W.; Oesterhelt, D. *Chem. Phys. Lett.* **1988**, *144*, 215.
(4) Du, M.; Fleming, G. R. *Biophys. Chem.* **1993**, *48*, 101.
(5) Mathies, R. A.; Brito Cruz, C. H.; Pollard, W. T.; Shank, C. V. *Science* **1988**, *240*, 777.
(6) Polland, H. J.; Franz, M. A.; Zinth, W.; Kaiser, W.; Kölling, E.; Oesterhelt, D. *Biophys. J.* **1986**, *49*, 651.
(7) Schoenlein, R. W.; Peteanu, L. A.; Mathies, R. A.; Shank, C. V. *Science* **1991**, *254*, 412.
(8) Sharkov, A. V.; Pakulev, A. V.; Chekalin, S. V.; Matveetz, Y. A. *Biochim. Biophys. Acta* **1985**, *808*, 94.
(9) Wang, Q.; Schoenlein, R. W.; Peteanu, L. A.; Mathies, R. A.; Shank, C. V. *Science* **1994**, *266*, 422.
(10) Becker, R. S.; Freedman, K. *J. Am. Chem. Soc.* **1985**, *107*, 1477.
(11) Freedman, K. A.; Becker, R. S. *J. Am. Chem. Soc.* **1986**, *108*, 1245.
(12) Koyama, Y.; Kubo, K.; Komori, M.; Yasuda, H.; Mukai, Y. *Photochem. Photobiol.* **1991**, *54*, 433.
(13) Huang, J. Y.; Chen, Z. P.; Lewis, A. *J. Phys. Chem.* **1989**, *93*, 3314.
(14) Mathies, R. A.; Stryer, L. *Proc. Nat. Acad. Sci. USA* **1976**, *73*, 2169.
(15) Ponder, M.; Mathies, R. A. *J. Phys. Chem.* **1983**, *87*, 5090.
(16) Groma, G. I.; Colonna, A.; Lambry, J. C.; Petrich, J. W.; Varo, G.; Joffre, M.; Vos, M. H.; Martin, J. L. *Proc. Nat. Acad. Sci. U. S. A.* **2004**, *101*, 7971.
(17) Colonna, A.; Groma, G. I.; Martin, J. L.; Joffre, M.; Vos, M. H. *J. Phys. Chem. B* **2007**, *111*, 2707.
(18) Xu, D.; Martin, C.; Schulten, K. *Biophys. J.* **1996**, *70*, 453.
(19) Kennis, J. T. M.; Larsen, D. S.; Ohta, K.; Facciotti, M. T.; Glaeser, R. M.; Fleming, G. R. *J. Phys. Chem. B* **2002**, *106*, 6067.
(20) Schenkl, S.; van Mourik, F.; van der Zwan, G.; Haacke, S.; Chergui, M. *Science* **2005**, *309*, 917.
(21) Heyne, K.; Herbst, J.; Dominguez-Herradon, B.; Alexiev, U.; Diller, R. *J. Phys. Chem.* **2000**, *104*, 6053.
(22) Nonella, M. *J. Comput. Chem.* **1997**, *18*, 677.
(23) Nonella, M. *J. Phys. Chem. B* **2000**, *104*, 11379.
(24) Schenkl, S.; van Mourik, F.; Friedman, N.; Sheves, M.; Schlesinger, R.; Haacke, S.; Chergui, M. *Proc. Nat. Acad. Sci. U. S. A.* **2006**, *103*, 4101.
(25) Song, L.; El-Sayed, M. A.; Lanyi, J. K. *Science* **1993**, *261*, 891.
(26) Hamm, P.; Zurek, M.; Röschinger, T.; Patzelt, H.; Oesterhelt, D.; Zinth, W. *Chem. Phys. Lett.* **1996**, *263*, 613.
(27) Hou, B.; Friedman, N.; Ruhman, S.; Sheves, M.; Ottolenghi, M. *J. Phys. Chem. B* **2001**, *105*, 7042.
(28) Hamm, P.; Zurek, M.; Röschinger, T.; Patzelt, H.; Oesterhelt, D.; Zinth, W. *Chem. Phys. Lett.* **1997**, *286*, 180.
(29) Zgrablić, G.; Voitchovsky, K.; Kindermann, M.; Haacke, S.; Chergui, M. *Biophys. J.* **2005**, *88*, 2779.
(30) Zgrablić, G.; Haacke, S.; Chergui, M. *Chem. Phys.* **2007**, *338*, 168.
(31) Hou, B. X.; Friedman, N.; Ottolenghi, M.; Sheves, M.; Ruhman, S. *Chem. Phys. Lett.* **2003**, *381*, 549.
(32) Childs, R. F.; Shaw, G. S. *J. Am. Chem. Soc.* **1988**, *110*, 3013.
(33) Prokhorenko, V. I.; Nagy, A. M.; Waschuk, S. A.; Brown, L. S.; Birge, R. R.; Miller, R. J. D. *Science* **2006**, *313*, 1257.
(34) Ruhman, S.; Hou, B. X.; Friedman, N.; Ottolenghi, M.; Sheves, M. *J. Am. Chem. Soc.* **2002**, *124*, 8854.
(35) Schmidt, B.; Sobotta, C.; Heinz, B.; Laimgruber, S.; Braun, M.; Gilch, P. *Biochim. Biophys. Acta-Bioenerg.* **2005**, *1706*, 165.
(36) Vengris, M.; van der Horst, M. A.; Zgrablic, G.; van Stokkum, I. H. M.; Haacke, S.; Chergui, M.; Hellingwerf, K. J.; van Grondelle, R.; Larsen, D. S. *Biophys. J.* **2004**, *87*, 1848.
(37) Zgrablić, G. Solvent effects on the ultrafast dynamics of the retinal chromophore of bacteriorhodopsin, Ecole Polytechnique Fédérale de Lausanne, 2006.
(38) Cannizzo, A.; Bram, O.; Zgrablic, G.; Tortschanoff, A.; Oskouei, A. A.; van Mourik, F.; Cherguil, M. *Opt. Lett.* **2007**, *32*, 3555.
(39) Lakowicz, J. R. *Principles of Fluorescence Spectroscopy*, 2 ed.; Klewer Academic/Plenum Publishers: New York, 1999.
(40) Förster, T. *Fluoreszenz Organischer Verbindungen*; Vandenhoeck & Ruprecht: Göttingen, 1951.
(41) Mataga, N.; Kubota, T. *Molecular Interactions and Electronic Spectra*; Marcel Dekker, Inc.: 1970.
(42) Birge, R. B.; Zhang, C.-F. *J. Chem. Phys.* **1990**, *92*, 7178.
(43) Chizhov, I.; Schmies, G.; Seidel, R.; Sydor, J. R.; Luttenberg, B.; Engelhard, M. *Biophys. J.* **1998**, *75*, 999.
(44) Metzler, D. E. *Vision Res.* **1978**, *18*, 1417.
(45) Scharnagl, C.; Fischer, S. F. *Chem. Phys.* **1996**, *212*, 231.
(46) Bachilo, S. M.; Bondarev, S. L.; Gillbro, T. *J. Photochem. Photobiol. B* **1996**, *34*, 39.
(47) Bachilo, S. M.; Gillbro, T. *J. Phys. Chem. A* **1999**, *103*, 2481.
(48) Baasov, T.; Sheves, M. *J. Am. Chem. Soc.* **1985**, *107*, 7524.
(49) Fee, R. S.; Maroncelli, M. *Chem. Phys.* **1994**, *183*, 235.
(50) Schenkl, S.; Portuondo, E.; Zgrablic, G.; Chergui, M.; Haacke, S.; Friedman, N.; Sheves, M. *Phys. Chem. Chem. Phys.* **2002**, *4*, 5020.
(51) Schenkl, S.; Zgrablic, G.; Portuondo-Campa, E.; Haacke, S.; Chergui, M. *Chem. Phys. Lett.* **2007**, *441*, 322.
(52) Birge, R. R.; Murray, L. P.; Zidovetzki, R.; Knapp, H. M. *J. Am. Chem. Soc.* **1987**, *109*, 2090.
(53) Lippert, E. *Z. Naturforsch., A: Phys. Sci.* **1955**, *10*, 541.
(54) Lippert, E. *Z. Elektrochem.* **1957**, *61*, 962.
(55) Mataga, N.; Kaifu, Y.; Koizumi, M. *Bull. Chem. Soc. Jpn.* **1955**, *28*, 690.
(56) Horng, M. L.; Gardecki, J. A.; Papazyan, A.; Maroncelli, M. *J. Phys. Chem.* **1995**, *99*, 17311.
(57) Lin, S. W.; Groesbeek, M.; van der Hoef, I.; Verdegem, P.; Lugtenburg, J.; Mathies, R. A. *J. Phys. Chem. B* **1998**, *102*, 2787.
(58) Smith, S. O.; Myers, A. B.; Mathies, R. A.; Pardoen, J. A.; Winkel, C.; van den Berg, E. M. M.; Lugtenburg, J. *Biophys. J.* **1985**, *47*, 653.
(59) Cembran, A.; Bernardi, F.; Olivucci, M.; Garavelli, M. *J. Am. Chem. Soc.* **2004**, *126*, 16018.
(60) Cembran, A.; Bernardi, F.; Olivucci, M.; Garavelli, M. *Proc. Nat. Acad. Sci. U. S. A.* **2005**, *102*, 6255.
(61) Kandori, H.; Sasabe, H. *Chem. Phys. Lett.* **1993**, *216*, 126.
(62) Logunov, S. L.; Song, L.; El-Sayed, M. A. *J. Phys. Chem.* **1996**, *100*, 18586.
(63) Olivucci, M.; Lami, A.; Santoro, F. *Angew. Chem., Int. Ed.* **2005**, *44*, 5118.
(64) González-Luque, R.; Garavelli, M.; Bernardi, F.; Merchán, M.; Robb, M. A.; Olivucci, M. *Proc. Nat. Acad. Sci.* **2000**, *97*, 9379.
(65) Kovalenko, S. A.; Schanz, R.; Hennig, H.; Ernsting, N. P. *J. Chem. Phys.* **2001**, *115*, 3256.

JP8077216